Plasmon excitations at diffuse interfaces

2008 J. Phys.: Condens. Matter 20 304205

(http://iopscience.iop.org/0953-8984/20/30/304205)

J. Phys.: Condens. Matter **20** (2008) 304205 (7pp) doi:10.1088/0953-8984/20/30/304205

Plasmon excitations at diffuse interfaces

A Howie[1], **F J Garcia de Abajo**[2] **and A Rivacoba**[3,4]

[1] Cavendish Laboratory, Madingley Road, Cambridge CB3 0HE, UK
[2] Instituto de Óptica-CSIC, Serrano 121, 28006 Madrid, Spain
[3] Donostia International Physics Travelling (DIPC) and Centro Mixto CSIC-UPV/EHU, Apartado 1072, 20080 San Sebastian, Spain
[4] Materialen Fisika Saila, Kimika Fakultatea, Apartado 1072, 20080 San Sebastian, Spain

E-mail: ah30@cam.ac.uk (A Howie)

Received 30 October 2007, in final form 17 December 2007
Published 8 July 2008
Online at stacks.iop.org/JPhysCM/20/304205

Abstract
Energy losses experienced by a fast electron probe moving through a dielectric medium have been studied both numerically and analytically, where the response function varies continuously with position in one transverse direction. The frequent assumption that the loss spectrum should exhibit a peak determined by the plasmon energy in a homogeneous medium with the composition found locally at the probe position can be incorrect. In free electron systems, inhomogeneous effects can cause spectral shape changes as well as peak shifts. Computations for diffuse interfaces between semiconductors with differing band gaps are also reported. Prospects for improved spatial resolution in valence loss spectroscopy at higher momentum transfer are discussed.

1. Introduction

For spatially localized spectroscopy, electron microscopists have generally favoured the core loss region because the data can be related quite directly to local chemical composition and even electronic structure. However the valence region has significant advantages because of the strength of the signal and the frequent occurrence of prominent peaks associated with the excitation of plasmons that can provide a simple connection to valence electron density or more generally a means of identifying specific local phases. Plasmon loss mapping has consequently attracted attention both in early pioneering work [1–4] and more recently [5, 6] but has proceeded on a local excitation assumption that the loss spectrum at each point is identical to that from a homogeneous medium with the same local composition. In this low energy and momentum transfer region, the problem of Coulomb delocalization is potentially significant and was first emphasized particularly vividly by the work of Echenique and Pendry [7] on the excitation of surface plasmons by an electron travelling outside a metal.

Detailed analytical theories of valence excitation have more recently been developed and tested for sharp interfaces with simple planar, cylindrical or spherical geometry and numerical approaches have been used for more complex geometries [8–10]. A general principle emerging from this work is that for each nanostructure there are plasmons or other characteristic valence excitation eigenmodes at energies determined by peaks in the imaginary parts of bulk or interface response functions. The excitation amplitude of each mode and hence its contribution to the energy loss spectrum depends on the trajectory (i.e., impact parameter of the fast electron used in the excitation). Furthermore the sum of these different mode contributions is often constant under changes in the impact parameter. This so-called begrenzungs effect is manifested most clearly in the case of excitations near a planar interface.

In other cases in which continuous changes rather than sharp interfaces may be present, electron microscopists continue to make their local excitation assumption ignoring any gradient corrections in the plasmon energies or in their excitation probabilities. Surface scientists have already addressed the influence on surface plasmon energies and dispersion of the details of the valence electron density profile at a free surface (see [12, 13] and references therein), but have not considered the more general variations of interest here nor have they included the details of the excitation process by the high energy electrons used in electron microscopy. Here we develop a general classical theory to handle situations where the dielectric response is a function of one spatial coordinate normal to the electron beam direction. The general spatial variation has to be solved numerically but we also note some special cases that admit analytical solution.

2. General theory

Consider a diffuse interface between two semi-infinite media with dielectric functions ϵ_1 and ϵ_2 (see figure 1(a)). In the

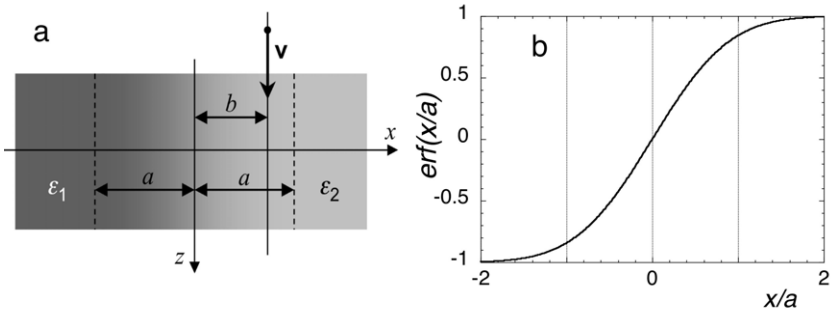

Figure 1. (a) Scheme for the diffuse interface between two media; (b) the erf(x/a) function used to model the transition region in the boundary.

direction x normal to the interface the diffuse region extends over a distance characterized by a length parameter a and within which the permittivity $\epsilon(x, \omega)$ is a continuous function of the position x. In this work we have employed two different profiles: a linear dependence of ϵ on x (this is solved analytically in section 3.1) and a more realistic smooth profile described by the error function erf(x/a) shown in figure 1(b). We study the energy loss experienced by a fast electron moving with velocity v in the z direction parallel to the interface, and with impact parameter b relative to the centre of the interfacial region.

The energy loss per unit length is related to the induced potential $\phi_{\text{ind}}(x, q, \omega)$, which can be obtained from Poisson's equation for a moving source charge $e\delta(x - b)\delta(y)\delta(z - vt)$. Making use of the translational invariance along the y and z axes, we can Fourier transform the potential from variables (x, y, z, t) to (x, q_y, q_z, ω) and write the Poisson equation in the form:

$$\frac{\mathrm{d}^2}{\mathrm{d}x^2}\phi(x, q, \omega) + \frac{1}{\epsilon}\left(\frac{\mathrm{d}\epsilon}{\mathrm{d}x}\right)\frac{\mathrm{d}}{\mathrm{d}x}\phi(x, q, \omega) - q^2\phi(x, q, \omega) = \frac{8e\pi^2}{\epsilon}\delta(x - b)\delta(q_z v - \omega), \tag{1}$$

where $q^2 = q_y^2 + q_z^2$, and q_y and q_z are the momentum components conjugate to the y and z coordinates. The rightmost delta function in equation (1) comes from energy conservation and ensures that only one value of $q_z = \omega/v$ arises, so we can from now on assume $q^2 = q_y^2 + (\frac{\omega}{v})^2$. The diffuse interface response is thus characterized by the dimensionless parameter qa which has a minimum value $\omega a/v$.

The general solution of equation (1) can be expressed in terms of the regular solutions $\phi_+(x, q, \omega) = \mathrm{e}^{-qx}$ for $x > a$ and $\phi_-(x, q, \omega) = \mathrm{e}^{qx}$ for $x < a$ in both homogeneous regions, which are then propagated through the inhomogeneous region up to $x = b$ (this can be done numerically for arbitrary dependence of $\epsilon(x, \omega)$ on x). Let $\phi_\pm(x, q, \omega)$ be the values of these solutions in the interface. The continuity of the potential at $x = b$ leads to the expression

$$\phi(x, q, \omega) = \begin{cases} A\phi_+(b, q, \omega)\phi_-(x, q, \omega), & x < b, \\ A\phi_-(b, q, \omega)\phi_+(x, q, \omega), & x > b, \end{cases}$$

where the normalization constant A is determined by imposing at $x = b$ the jump in the first derivative of $\phi(x, q, \omega)$ given by equation (1). One finds:

$$A = -\frac{8e\pi^2}{\epsilon(b, \omega)W(b, q, \omega)}\delta(q_z v - \omega), \tag{2}$$

where $W(b, q, \omega)$ is the Wronskian

$$W(b, q, \omega) = \phi_-(b, q, \omega)\frac{\mathrm{d}}{\mathrm{d}x}\phi_+(x, q, \omega)\Big|_{x=b} - \phi_+(b, q, \omega)\frac{\mathrm{d}}{\mathrm{d}x}\phi_-(x, q, \omega)\Big|_{x=b}.$$

The component of the slowing down force in the direction of the probe velocity evaluated at the probe position is the stopping power (i.e., the energy loss per unit length), which is given by

$$\frac{\mathrm{d}W}{\mathrm{d}z} = \frac{\mathrm{i}e^2}{\pi v^2}\int_{-\infty}^{\infty}\omega\,\mathrm{d}\omega\,\mathrm{d}q_y\frac{\phi_+(b, q, \omega)\phi_-(b, q, \omega)}{\epsilon(b, \omega)W(b, q, \omega)} = \int_0^\infty \omega\,\mathrm{d}\omega\frac{\mathrm{d}P(\omega)}{\mathrm{d}z},$$

where

$$\frac{\mathrm{d}P(\omega)}{\mathrm{d}z} = -\frac{2e^2}{\pi v^2}\int_0^\infty \mathrm{d}q_y\,\mathrm{Im}\left\{\frac{\phi_+(b, q, \omega)\phi_-(b, q, \omega)}{\epsilon(b, \omega)W(b, q, \omega)}\right\} \tag{3}$$

is the energy loss probability per unit length. The remainder of our paper will focus on this quantity, which is directly probed by EELS.

3. Analytical solutions

3.1. Dielectric function depending linearly on the position

Here we consider a dielectric function in the interface that is a linear function of position. Although the abrupt change of slope at the edge of the homogeneous regions may be somewhat unrealistic, the model can be analytically solved, providing a useful understanding of the role of the interface thickness a in the loss spectra. Our dielectric function is now given by

$$\epsilon(x, \omega) = \begin{cases} \epsilon_1(\omega), & x < -a, \\ \alpha(\omega) + \beta(\omega)\dfrac{x}{a}, & -a < x < a, \\ \epsilon_2(\omega), & x > a, \end{cases} \tag{4}$$

where

$$\alpha(\omega) = \tfrac{1}{2}[\epsilon_1(\omega) + \epsilon_2(\omega)]$$

and

$$\beta(\omega) = \tfrac{1}{2}[\epsilon_2(\omega) - \epsilon_1(\omega)].$$

Using the non-dimensional complex variable $t(x,\omega) = qa\epsilon(x,\omega)\beta(\omega)^{-1}$, equation (1) in the interface becomes:

$$t^2\frac{\mathrm{d}^2}{\mathrm{d}t^2}\phi(t,q,\omega) + t\frac{\mathrm{d}}{\mathrm{d}t}\phi(t,q,\omega) - t^2\phi(t,q,\omega) = -\frac{8e\pi^2 at}{\beta}\delta(t-t_b)\delta(q_z v-\omega), \tag{5}$$

where we have defined $t_b = t(b,\omega)$. When the probe trajectory lies in one of the homogeneous regions (e.g., $b > a$), the solution of the homogeneous equation (5) in the interfacial region can be written as

$$\phi(t,q,\omega) = B(q,\omega)I_0(t) + C(q,\omega)K_0(t), \quad -a < x < a, \tag{6}$$

where K_0 and I_0 are modified Bessel functions [14]. Outside the interface the potential reduces to

$$\phi(t,q,\omega) = \begin{cases} A(q,\omega)\mathrm{e}^{qx}, & x < -a \\ \dfrac{4e\pi^2}{q\epsilon_2(\omega)}\mathrm{e}^{-q|x-b|}\delta(\omega - q_z v) & \\ \quad + D(q,\omega)\mathrm{e}^{-qx}, & x > a, \end{cases} \tag{7}$$

where A, B, C and D are functions determined by the continuity of the potential and the normal displacement at the edges of the interface ($x = \pm a$). After some tedious algebra the coefficient $D(q,\omega)$, needed to obtain the potential induced at the position of the electron, is found to be

$$D(x,q,\omega) = \frac{4e\pi^2}{q\epsilon_2}\mathrm{e}^{q(2a-b)}\delta(\omega - q_z v)\Pi(q,\omega), \tag{8}$$

where

$$\Pi(q,\omega) = \frac{\Delta I^{(-)}(t_2)\Delta K^{(+)}(t_1) - \Delta I^{(-)}(t_1)\Delta K^{(+)}(t_2)}{\Delta I^{(+)}(t_2)\Delta K^{(+)}(t_1) - \Delta I^{(-)}(t_1)\Delta K^{(-)}(t_2)}, \tag{9}$$

the coefficients $\Delta I^{(\pm)}$ and $\Delta K^{(\pm)}$ are defined as

$$\Delta I^{(\pm)}(t_i) = I_0(t_i) \pm I_1(t_i)$$

$$\Delta K^{(\pm)}(t_i) = K_0(t_i) \pm K_1(t_i)$$

and $t_i = qa\beta^{-1}\epsilon_i$ ($i = 1, 2$). The energy loss probability per unit length can be written in terms of $\Pi(q,\omega)$ as

$$\frac{\mathrm{d}P(\omega)}{\mathrm{d}z} = \frac{e^2}{\pi v^2}\int\frac{\mathrm{d}q_y}{q}\mathrm{Im}\left\{\frac{-1}{\epsilon_2} - \frac{\mathrm{e}^{2q(a-b)}}{\epsilon_2}\Pi(q,\omega)\right\}. \tag{10}$$

Equation (10) is an exact solution valid for any interface with dielectric function varying linearly between two regions of constant dielectric function. The first term is the well known expression of the energy loss probability per unit length of a probe moving in a homogeneous medium. The second one is the interface correction to the local bulk loss spectrum and represents a contribution from the excitation of interface plasmons and a related reduction in the local bulk loss probability. The exponential dependence on the impact parameter relative to the edge agrees with the dependence found in the general EELS theory for sharp interfaces.

Although equation (10) is not particularly transparent, it allows investigation of the role played by different q contributions to the overall loss spectrum, in connection with the sharpness of the interface. Assuming that $\epsilon(x,\omega)$ does not vanish (i.e., that at the plasmon energy it has a non-negligible imaginary part), one can use the series expansions of the Bessel functions to calculate the small q contribution ($qa \ll 1$) to the loss probability

$$\frac{1}{\epsilon_2}\Pi(q,\omega) \sim \left[\frac{-1}{\epsilon_2} - \frac{-2}{\epsilon_1+\epsilon_2}\right] \times \frac{1 - \frac{qa}{\beta}[\frac{1}{2}(\epsilon_1+\epsilon_2) - \frac{\epsilon_1\epsilon_2}{\epsilon_2-\epsilon_1}\ln\frac{\epsilon_2}{\epsilon_1}]}{1 + \frac{qa}{\beta}[\frac{1}{2}(\epsilon_2-\epsilon_1) + \frac{\epsilon_1\epsilon_2}{\epsilon_2+\epsilon_1}\ln\frac{\epsilon_2}{\epsilon_1}]}. \tag{11}$$

In the limit $qa \to 0$, equation (11) reproduces the surface term corresponding to a sharp interface. The term in $\mathrm{Im}\{\epsilon_2^{-1}\}$ describes a negative correction to the bulk excitation probability arising from the presence of the interface: this is the well known begrenzungs effect first found in thin films by Ritchie [15]. The second term corresponds to the excitation of surface plasmons, given by the condition $\mathrm{Re}\{\epsilon_1 + \epsilon_2\} \approx 0$.

In figure 2, we show the response function of the interface $\mathrm{Im}\{\epsilon_2^{-1}\Pi(q,\omega)\}$ for a 100 keV electron moving in the right side of an Al–Mg interface. Drude dielectric functions

$$\epsilon(\omega) = 1 - \frac{\omega_\mathrm{p}^2}{\omega(\omega + \mathrm{i}\gamma)} \tag{12}$$

with bulk plasmon energies $\hbar\omega_\mathrm{p} = 15.3$ eV (Al) and $\hbar\omega_\mathrm{p} = 10.6$ eV (Mg) have been considered for both media, and a constant value of the damping has been used throughout ($\hbar\gamma = 1$ eV). To allow comparison with the case of a sharp interface we have added its corresponding response function $\mathrm{Im}\{\epsilon_2^{-1} - 2(\epsilon_2+\epsilon_1)^{-1}\}$. The dependence of the response function on qa is twofold: on one hand the intensity decreases as qa increases, and on the other hand the interfacial peak shifts toward the local bulk plasmon energy. Both effects are a consequence of the fact that increasing q acts to reduce the size of the region scanned by the q component of the field, and therefore the contrast between the dielectric function in this region is weaker.

Note that in a typical electron microscope the minimum momentum $q_\mathrm{min} = \omega/v$ is of the order of 0.1 nm^{-1} and therefore the suitability of equation (11) is restricted to fairly sharp interfaces, and in the low momentum transfer range. Convenient interfaces for study might be those in polar media which on energy grounds may not be atomically or electronically sharp [16].

This Bessel function solution can be adapted to the case of probe trajectories inside the interface by using on either side of the probe position different solutions of the form of equation (6).

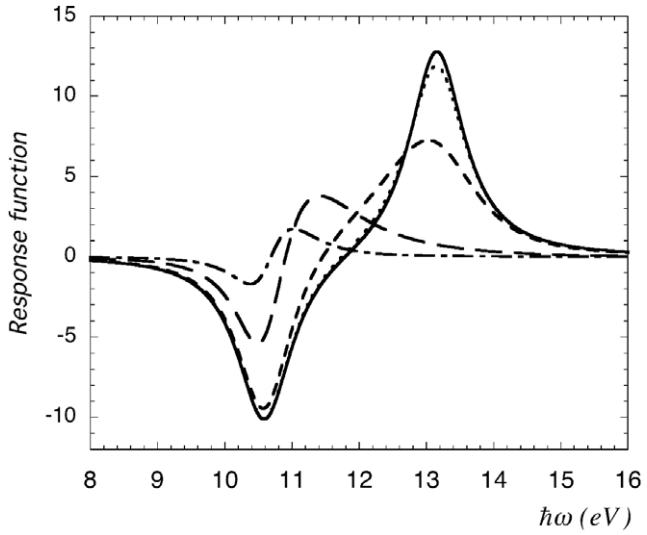

Figure 2. Response function of an interface with a linearly-dependent dielectric function $\epsilon(x, \omega)$ for four different values of qa: (. . . . . .) $qa = 0.01$, (- - - -) $qa = 0.1$, (— — —) $qa = 1$ and (— · —) $qa = 5$. The full line (——) corresponds to the sharp interface.

3.2. WKB method

We can obtain further insight by recasting equation (1) into a form where a WKB-like solution can be examined [11]. We change to the function

$$\Psi(x, q, \omega) = \epsilon(x, \omega)^{-\frac{1}{2}}\phi(x, q, \omega), \tag{13}$$

which outside the probe position satisfies the homogeneous equation

$$\frac{\mathrm{d}^2}{\mathrm{d}x^2}\Psi(x, q, \omega) - G(x, q, \omega)^2\Psi(x, q, \omega) = 0, \tag{14}$$

where

$$G(x, q, \omega)^2 = q^2 - \left[\frac{1}{2\epsilon(x, \omega)}\frac{\mathrm{d}\epsilon(x, \omega)}{\mathrm{d}x}\right]^2 + \frac{1}{2\epsilon(x, \omega)}\frac{\mathrm{d}^2\epsilon(x, \omega)}{\mathrm{d}x^2}. \tag{15}$$

Assuming that the permittivity varies slowly in the interface, so that the behaviour of G is ruled mainly by the q^2 term, the regular WKB solutions are

$$\Psi_{\pm}(x, q, \omega) = \frac{\mathrm{e}^{\mp\int G\mathrm{d}x}}{[\epsilon(x, \omega)G(x, q, \omega)]^{1/2}}. \tag{16}$$

Substituting these values in equation (3) one obtains

$$\frac{\mathrm{d}P(\omega)}{\mathrm{d}z} = -\frac{e^2}{\pi v^2}\int_{-\infty}^{\infty}\mathrm{d}q_y\,\mathrm{Im}\left\{\frac{1}{\epsilon(b, \omega)q\sqrt{1-(q\lambda)^{-2}}}\right\}, \tag{17}$$

where the constant

$$\lambda = \left\{\left[\frac{1}{2\epsilon(b, \omega)}\frac{\mathrm{d}\epsilon(x, \omega)}{\mathrm{d}x}\bigg|_{x=b}\right]^2 - \frac{1}{2\epsilon(b, \omega)}\frac{\mathrm{d}^2\epsilon(x, \omega)}{\mathrm{d}x^2}\bigg|_{x=b}\right\}^{-1/2} \tag{18}$$

can be interpreted as the length required to yield a significant change in the dielectric function. In the limit $q\lambda \gg 1$ this equation reduces to

$$\frac{\mathrm{d}P(\omega)}{\mathrm{d}z} = \frac{e^2}{\pi v^2}\,\mathrm{Im}\left\{\frac{-1}{\epsilon(b, \omega)}\right\}\int_{-\infty}^{\infty}\frac{\mathrm{d}q_y}{q} + \frac{e^2}{2\pi v^2}\,\mathrm{Im}\left\{\frac{-\lambda^{-2}}{\epsilon(b, \omega)}\right\}\int_{-\infty}^{\infty}\frac{\mathrm{d}q_y}{q^3}. \tag{19}$$

The first term is the usual expression describing local bulk plasmon excitation, while the second one provides a weak gradient correction with additive contributions from the square of the gradient and from the second derivative or curvature. In fact it can readily be seen that, in cases where the local bulk plasmon excitation function is symmetrical about the peak position, the loss peak will not be shifted by the first of these two correction terms, although it may be reduced in height and broadened. The WKB approximation may still be useful in more rapidly varying situations where the loss function has a high damping or when q-dependent spectroscopy is employed to select only larger values of q_y. In many cases of interest however, particularly of less diffuse interfaces, the simple WKB approximation used here will not be valid. The function G in equation (15) may even change sign leading to opposite curvature or even to oscillations of the potential in critical regions.

4. Numerical results

4.1. Free electron interfaces

Smooth interfaces between good conductor regions can be mimicked by the simple Drude dielectric response function of equation (12), modified to include a one-dimensional variation of the valence electron density $n(x)$, with the corresponding free electron plasmon frequency $\omega_\mathrm{p} = (4\pi ne^2/m)^{1/2}$.

Figure 3 shows computed loss spectra for 100 keV ($v =$ 75.1 au) electrons travelling parallel to an interface between Al (left side corresponding to negative impact parameters) and Mg. Dielectric functions of both homogeneous media are described by parameters as specified in section 3.1. The interface width is about 100 au (i.e., $a = 2.7$ nm) with a valence electron density profile given by the erf function shown in figure 1(b). Equation (3) has been numerically integrated up to a cut-off q_c in the integration variable q_y, which is directly related to the scattering acceptance semi-angle in the direction parallel to the interface θ_c according to $\hbar q_c = mv\sin\theta_\mathrm{c}$. In this figure we compare the actual loss spectra at the centre ($b = 0$) and near the edges of the interface with the loss probability corresponding to a homogeneous medium described by a local dielectric function $\epsilon(b, \omega)$ (i.e., that at the position of the electron). The computed interface spectra exhibit a plasmon peak lower than in the homogeneous case but with a corresponding increase in width consistent with the begrenzungs effect.

As noted above on general grounds, there is no shift of the plasmon loss peak in the central, approximately linear, region. However in the regions where there is curvature in the profile plot, the position of the plasmon is shifted

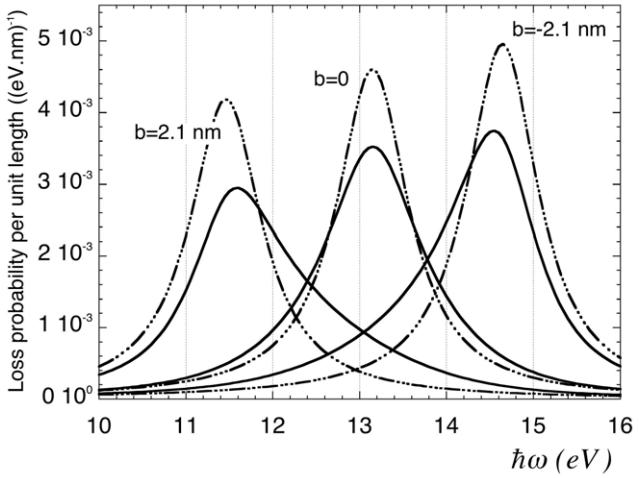

Figure 3. EEL spectra for 100 keV electrons travelling parallel to an Al–Mg interface, for three different beam trajectories. The solid lines correspond to the spectra in the diffuse interface with $a = 2.7$ nm. Broken lines spectra correspond to a homogeneous medium of dielectric function $\epsilon(b, \omega)$. The cut-off in q_y corresponds to a collecting aperture $\theta_c = 1$ mrad in the direction parallel to the interface (y).

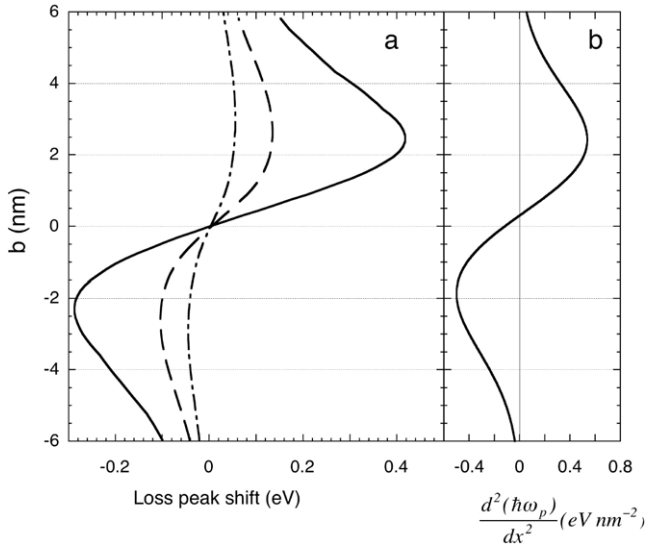

Figure 4. (a) Shift in the loss peak energy as a function of the beam position. Three cut-off upper limits on q_y integration corresponding to $\theta_c = 0.1$ mrad (——), $\theta_c = 1$ mrad (– – –) and $\theta_c = 10$ mrad (— · —), have been considered. Plot (b) shows the second spatial derivative of the local plasmon energy along the interface.

toward the values of the central plasmon peak, i.e., toward the position where an interface plasmon would appear for a sharp interface. This peak shift is shown in figure 4 for three different cut-off values q_c showing a roughly linear dependence on $\mathrm{d}^2\omega_\mathrm{p}/\mathrm{d}x^2$ (and indeed also on $\mathrm{d}^2\omega_\mathrm{p}^2/\mathrm{d}x^2$). In accordance with the above discussion, the peak shift is much more pronounced for small values of q_y. For these free electron situations, the delocalization parameter $[q\lambda(x, \omega)]^{-2}$ employed in equation (17) and evaluated at the peak frequency $\omega = \omega_\mathrm{p}(x)$ takes the form

$$[q\lambda(x,\omega)]^{-2} = \frac{-1}{q^2}\left\{\frac{1}{4\omega_\mathrm{p}(x)^2\gamma^2}\left[\frac{\mathrm{d}\omega_\mathrm{p}^2}{\mathrm{d}x}\right]^2 + \frac{\mathrm{i}}{\omega_\mathrm{p}(x)\gamma}\frac{\mathrm{d}^2\omega_\mathrm{p}^2}{\mathrm{d}x^2}\right\}. \qquad (20)$$

At the minimum momentum transfer $q_\mathrm{min} = \omega/v = 0.14\,\mathrm{nm}^{-1}$ (inside Al), the magnitude of each of the terms in the right-hand side of equation (20) exceeds unity over much of the profile shown in figure 3, so that we are well outside the range of the WKB approximation. Nevertheless our computations indicate that the peak displacement is still proportional to the second term including its dependence on q and γ. The dependence on q_c is less marked since this reflects an average over a range of q_y.

4.2. Semiconductor interface

To provide a simple model of a diffuse interface between two semiconductors with different band gaps $\hbar\omega_g$ but the same valence electron density n, we employ the response function

$$\epsilon(x,\omega) = 1 + \frac{4\pi ne^2m^{-1}}{\omega_g(x)^2 - \omega(\omega + \mathrm{i}\gamma)}. \qquad (21)$$

In particular, we chose a valence electron density with $\hbar[4\pi ne^2/m]^{1/2} = 17$ eV, band gaps $\hbar\omega_{1g} = 1$ eV and $\hbar\omega_{2g} = 3$ eV with a continuous erf variation between these values across the diffuse boundary region of half width $a = 2.7$ nm, and a damping parameter $\hbar\gamma = 0.1$ eV.

As in the local approximation, the bulk loss near 17 eV is only very slightly influenced by the band gap and does not exhibit any significant variation across the interface. The well known interface plasmon arises at 2.2 eV between the two band edges where $\epsilon_1(\omega) + \epsilon_2(\omega) \approx 0$ and, being dependent on the dielectric contrast between the two media, will be completely absent in any local excitation model. As shown in figures 5(a) and (b), the height of the peak is much lower for a diffuse interface than for a sharp one. Quantitative measurements of interface loss peak intensities may therefore offer the best means of addressing the sharpness of the interface, although the dependence on aperture size (or cut-off wavevector q_c) should be noted. For the sharp interface (figure 5(b)), the peak intensity at $b = 0$ shows the familiar logarithmic dependence on aperture size or cut-off wavevector, in contrast to the diffuse interface (figure 5(a)), in which this dependence weakened at higher q values. This behaviour stems from the low value of $\omega a/v = 0.06$, which means that the interface loss is excited over a large range of impact parameters corresponding predominantly to low-q transfers. This effect is more significant at the plasmon peak frequency, thus giving rise to a pronounced broadening of the observed loss feature.

5. Discussion

Our results suggest that for a typical objective aperture of 10 mrad a shift in the free electron plasmon peak of $\Delta(\hbar\omega_\mathrm{p}) = 0.05$ eV could be induced by a curvature $\mathrm{d}^2(\hbar\omega_\mathrm{p})/\mathrm{d}x^2 = 0.4$ eV nm^{-2} with a rough proportionality between these quantities. This correction would be too small to have any effect on the slowly varying valence density profiles studied

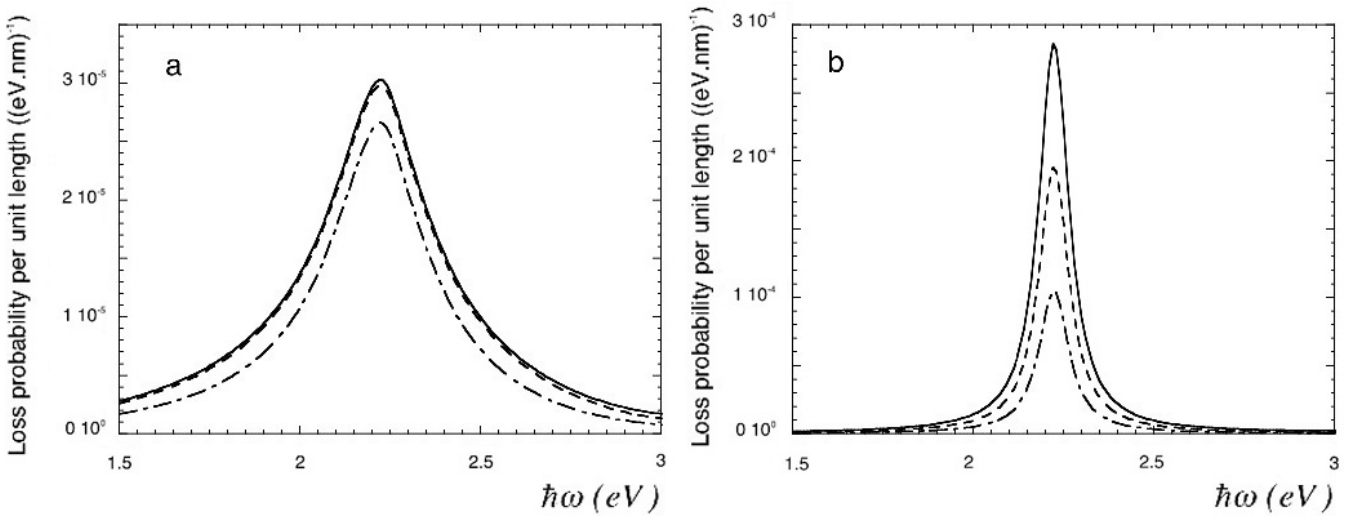

Figure 5. EEL spectra in a diffuse (a) and sharp (b) interface between two semiconductors with band energies $\hbar\omega_{1g} = 1$ eV and $\hbar\omega_{2g} = 3$ eV. The impact parameter is $b = 0$ and the probe energy 100 keV. Three collecting apertures in the direction parallel to the interface have been considered: $\theta_c = 0.1$ mrad (— · —), $\theta_c = 1$ mrad (- - - -) and $\theta_c = 10$ mrad (——). The diffuse interface has $a = 2.7$ nm.

in early work [1–4], although the changes in peak shape could invalidate more general adoption of the method used there to detect extremely small changes in ω_p. Curvature corrections could well be non-negligible in current observations of more rapidly varying situations. Observed changes in peak height or shape might then be a useful indicator of the need for gradient and curvature corrections to the local model. Our computations on interface plasmons in semiconductors highlight a sensitivity to interface diffuseness which should be more easily detectable. Relativistic corrections, which we have ignored, are however more likely to be significant in this situation [17] than would be expected for bulk plasmon excitation in metals.

The methods presented here can yield spectra for any assumed model of a one-dimensional dielectric profile. Ideally of course we would prefer to have a solution to the inverse problem of deducing directly the dielectric profile from the collected valence loss spectra. In the absence of such a procedure the best option is probably to start with a profile obtained from the local valence excitation model supplemented by imaging or core loss spectroscopy information. This profile could then be adjusted by trial and error methods to improve consistency with the observed valence loss spectra and those computed as described here.

Although the classical theory agrees with quantum theory provided all inelastically scattered electrons are collected [19] it gives only approximate results for each value of q. Nevertheless it is clear that the corrections to the local model are smallest for large values of q, which raises the possibility of carrying out *momentum-selected spectroscopy*. The usual circular objective aperture, imposing an axial cut-off q_a, axially limits the Fourier range of loss probability as a function of x to values of $q_x < [q_a^2 - q_y^2]^{1/2}$. Within the restrictions of classical excitation theory, this effect can be modelled by a further Fourier transform of our data [17]. Another option, already explored as a route to higher spatial resolution in

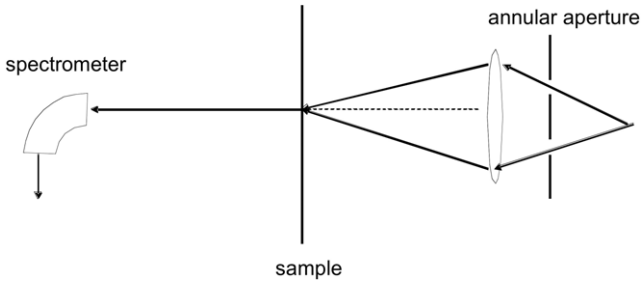

Figure 6. Sketch of a hollow cone electron beam illumination set-up for collection of high momentum transfers.

valence EELS [18], is to work with a spectrometer collection aperture displaced in the q_y direction to select only high values of q with less need for non-local corrections but at the expense of reduced signal strength. This simple displaced-aperture procedure would of course be suitable only for dielectric variations in only one dimension. To obtain high spatial resolution more generally in valence excitation, it might be easiest to resort to hollow cone illumination in STEM mode with a relatively smaller axial spectrometer collecting aperture as indicated in figure 6. With aberration correction, the hollow cone semi-angle could be as much as 40 mrad, giving potential spatial resolution on the unit cell or even sub-unit cell level. For such large values of q, the direct valence excitations would be well outside the plasmon excitation region and would be concentrated near the Bethe ridge energy $q^2/2m$. Plasmon loss electrons could still obviously reach the spectrometer by additional large elastic or quasi-elastic scattering processes. By tuning the spectrometer to accept a range of energies in the Bethe ridge region, but still avoiding core losses on the one hand and plasmon losses on the other, it might be possible to access valence bond geometries by such a Bethe ridge mapping procedure.

It would be useful to improve the theory to take more exact account of each momentum transfer $\hbar q$. The effects

of dispersion should also be included in developing a more accurate theory of plasmon excitation in inhomogeneous situations.

Acknowledgments

A Howie thanks Professor P Echenique and the staff of the Donostia International Physics Centre for excellent stimulation and hospitality. This work was supported in part by the Spanish MEC (contract No. FIS2004-06490-C03-02) and by the EU (project No. STRP-016881-SPANS).

References

[1] Cundy S L, Metherell A J F, Whelan M J, Unwin P N T and Nicholson R B 1968 *Proc. R. Soc.* A **307** 267–81
[2] Cundy S L, Metherell A J F and Whelan M J 1968 *Phil. Mag.* **17** 141
[3] Spalding D R, Villagrana R E and Chadwick G A 1969 *Phil. Mag.* **20** 471
[4] Spalding D R 1976 *Phil. Mag.* **34** 1073
[5] Sigle W, Krämer S, Varshney V, Zern A, Eigenthaler U and Rühle M 2003 *Ultramicroscopy* **96** 565–71
[6] Daniels H R, Brydson R, Brown A and Rand B 2003 *Ultramicroscopy* **96** 547
[7] Echenique P M and Pendry J B 1975 *J. Phys. C: Solid State Phys.* **8** 2936
[8] Howie A 1999 *Topics in Electron Diffraction and Microscopy of Materials* ed P B Hirsch (Bristol: IOP Publishing) pp 79–107
[9] Rivacoba A, Zabala N and Aizpurua J 2000 *Prog. Surf. Sci.* **65** 1–64
[10] Lambin Ph, Henrard L, Thiry P, Silien C and Vigneron J P 2003 *J. Electron Spectrosc.* **129** 281–92
[11] Morse P and Feshbach H 1953 *Methods of Theoretical Physics* vol 2 (New York: McGraw-Hill) pp 1092–5
[12] Quinn J J 1995 *Nucl. Instrum. Methods* B **96** 460–4
[13] Ford G W and Weber W H 1984 *Phys. Rep.* **113** 195
[14] Abramowitz M and Stegun I A 1964 *Handbook of Mathematical Functions* (New York: Dover)
[15] Ritchie R H 1957 *Phys. Rev.* **106** 874
[16] Nakagawa N, Hwang H Y and Muller D A 2006 *Nat. Mater.* **5** 204
[17] Moreau P, Brun N, Walsh C A, Colliex C and Howie A 1997 *Phys. Rev.* B **56** 6774
[18] Muller D A and Silcox J 1995 *Ultramicroscopy* **59** 195
[19] Ritchie R H 1981 *Phil. Mag.* A **44** 931